IRO Journal on Sustainable Wireless Systems (ISSN: 2582-3167)
www.irojournals.com/irosws/

Corner Perturbation-Enabled Dual-Resonant Circularly Polarized Antenna for Resilient UAV Networks

Ramesh S.[1], Dillip Prasad P.[2], Gokulvasan V.[3], Guna Sekar G.[4], Gokul J.[5]

Department of Electronics and Communication Engineering, SRM Valliammai Engineering College, Tamil Nadu, India.

E-mail: [1]rameshs.ece@srmvalliammai.ac.in, [2]dillipprasad353@gmail.com, [3]gokulvasanv6@gmail.com, [4]gunagopi2310@gmail.com, [5]gokuljaga04@gmail.com

Abstract

In this paper, the development process of a miniature dual-band CP (circularly polarized) microstrip patch antenna is presented for wireless onboard communication in unmanned aerial vehicles (UAVs). It is designed to work in 2.4GHz and 5.2GHz ISM (industrial, scientific, and medical) Wi-Fi bands for achieving high spectral efficiency and communication reliability for critical UAV applications like autonomous monitoring, swarm operations, and emergency communications. The CP radiation technique is used in order to eliminate polarization loss as it is sensitive to the different orientations of aerial platforms. The proposed antenna is composed of an integrated U-slot and two stubs and has asymmetrical corners for obtaining orthogonal modal excitation required for CP operation. A DGS (defected ground structure) cell is also embedded to extend the bandwidth range. The proposed antenna is made up of a FR-4 dielectric substrate, with a compact footprint of 48 × 39 × 1.6 mm³. According to electromagnetic modeling studies, the highest realized gain for the proposed antenna occurs at 3.29 dBi at 2.4 GHz and 2.54 dBi at 5.2 GHz, with impedance bandwidths of 163 MHz and 600 MHz, respectively.

Keywords: Axial Ratio, Circular Polarization, Corner Perturbation, Defected Ground Structure, Dual-Band Patch Antenna, U-slot.

DOI: https://doi.org/10.36548/jsws.2026.3.001
Extended version of article received from **6th International Conference on Artificial Intelligence, 6G Communications and Network Technologies 2026**
Received: 12.04.2026, received in revised form: 17.05.2026, accepted: 04.06.2026, published: 16.06.2026

1. Introduction

The widespread usage of UAVs in both civil and military applications has created new constraints for the antenna systems needed to ensure reliable communication. Applications such as precision farming, search & rescue missions, bridge inspection, or even swarm formation have led to the need for compact and lightweight aerial transceivers that exhibit predictable and constant radiation characteristics throughout their entire range of motion [1]. In contrast to static wireless platforms, the antenna systems used in UAVs experience constant rotations in terms of roll, pitch, and yaw motions, which leads to occasional misalignment of the antenna radiation pattern with polarization losses [1].

The inclusion of antennas on small airframes raises the level of difficulty in antenna design. An ideal antenna will need to be highly efficient in terms of its volume, maintain an optimal shape without disturbing aerodynamics, provide stable radiation patterns in various conditions, and reduce electromagnetic interference with other metal elements [2]. Creating a circular polarization system based on a single-feed microstrip system requires the simultaneous excitation of two modes in the antenna at equal amplitudes with a phase difference of 90° between them [4]. Several methods for designing dual band and circularly polarized microstrip antennas have been proposed in past research efforts. Akhter et al. [6] have studied a dual mode circular patch that operates at both 2.4 GHz and 5.2 GHz through hybrid modal excitations via a single coaxial connector. This antenna, fabricated using a low loss substrate by Rogers Corp., used parasitic elements to increase the impedance bandwidth and improve gain, giving it measured broadside gain greater than 9 dBi [5]. M. Ahmad et al. [16] studied square patch corner truncated antennas at 2.4 GHz, where they showed that geometric distortion of patches at diagonally opposite corners can separate the degenerate patch modes resulting in right hand circular polarization.

Yang and Lin [3] proposed a small-sized planar Wi-Fi antenna, which had dimensions of 16.5 x 30.3 x 1.6 mm³ and was tailored for dual-band operation at frequencies of 2.4 GHz and 5.8 GHz. It showed excellent performance characteristics with impedance bandwidths of 2.11-2.58 GHz and 5.06-7.5 GHz with $|S11| \leq -10$ dB to ensure efficient power transfer. Crucially, it ensured quasi-omnidirectional radiation at 2.4 GHz, providing reliable connections in open spaces, and end-fire radiation at 5.8 GHz oriented downward in the direction of the UAV for improved connectivity in an urban environment [7].

The vertically polarized radiation also guaranteed efficient communication at large distances. Thus, proper radiation pattern optimization is vital to improve the quality of UAV communications. Unmanned Aerial Vehicles (UAVs) have found their application in many fields, such as surveillance, disaster management, and smart city monitoring, and they require antennas, which would be not too bulky and would support reliable communication at various distances [8]. While patch antennas are popular due to their simple structure, they are often associated with limited bandwidth, poor polarization stability, and lower efficiency due to frequent orientation changes of the UAV during flights.

As a result of these challenges, we are proposing the use of a modified dual-resonant circularly polarized microstrip patch antenna that will be implemented using various changes to the design. This involves using a U slot to enable the creation of a dual band system, where corner perturbation and truncation methods will help control current distribution and improve circular polarization properties [9]. Impedance matching and bandwidth improvement are achieved using the stub loading technique, which, in addition, helps reduce surface waves using the defected ground structure. By implementing this design approach, it is anticipated that there will be increased bandwidth and polarization purity that will facilitate resilient UAV communication network implementation [10].

This research is structured as follows: Section 2 presents the Design and Structural Configuration of the Simulated Antenna. Section 3 discusses the simulated performance of Antenna parameters, including return loss, gain, and radiation characteristics, along with detailed analysis. Section 4 describes the fabrication process of the proposed antenna using an FR-4 substrate and provides the experimental results obtained from the fabricated prototype and discusses the observed performance which also presents a comparative validation between simulated and measured results to evaluate the consistency and effectiveness of the proposed design.

2. Design and Structural Configuration of the Simulated Antenna

All structural components of the 48 × 39 × 1.6 mm² antenna geometry are designed to function as an integrated system that achieves dual-band resonance and circular polarization within a single planar layer as shown in Figure 1(a) and 1(b). At 2.4 GHz, the patch element supports its TM_{10} and TM_{01} fundamental modes. Applying asymmetric triangular truncations at two diagonally opposing corners designated TL and TH breaks the modal degeneracy and

introduces a controlled 90° phase shift between the two orthogonal field components, which is the necessary condition for circularly polarized radiation [11].

The reactive stubs placed at the remaining two corners (LL and RL) serve a dual function: stabilizing the polarization purity and providing secondary impedance tuning at the lower band. At 5.2 GHz, the U-shaped slot etched onto the patch surface introduces an elongated current circulation path; the electrical length of this path is tuned to match one guided wavelength at the upper resonant frequency, which produces the second dip in the S_{11} response [12].

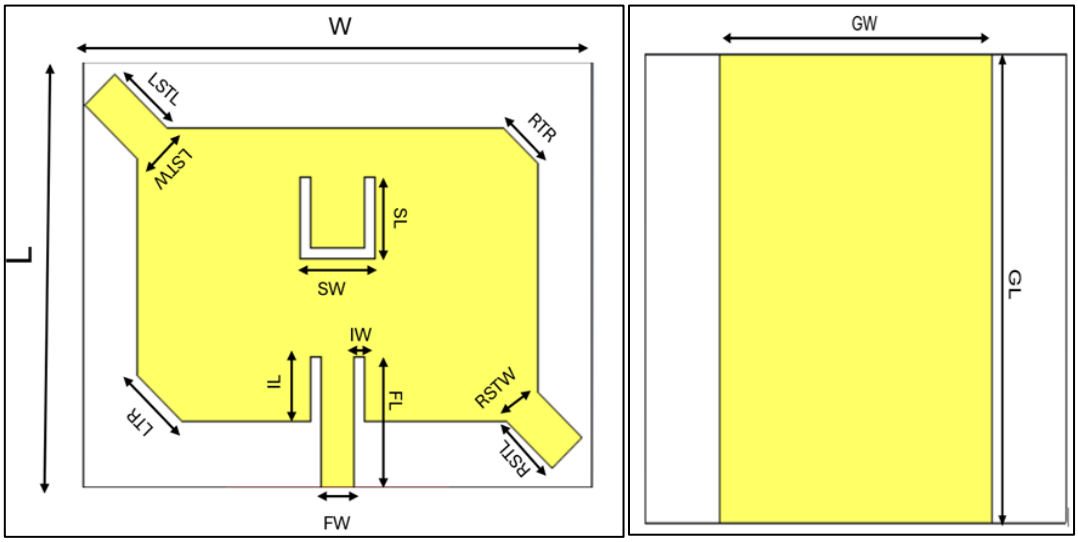

(a) (b)

Figure 1. (a) Simulated Antenna Top View, (b) Simulated Antenna Back View

The stubs concurrently reshape the surface current distribution at 5.2 GHz to sustain the amplitude balance and phase quadrature needed for CP at the upper band. The truncated ground plane on the reverse face reduces surface-wave excitation and widens the impedance bandwidth at both frequencies, while the inset-fed microstrip line couples' electromagnetic energy into the radiating patch through an impedance-matched notch [17]. The coordinated operation of all five design elements patch, corner truncations, stubs, U-slot, and partial ground within a compact single-layer FR-4 platform constitutes the central design contribution of this work. Table 1 shows the Optimized dimensional parameters of the simulated antenna.

Table 1. Optimized Dimensional Parameters of the Simulated Antenna

Parameters	Description	Values (in mm)
Frequencies	Operating Frequencies	2.4 & 5.2 GHZ
W	Substrate Width	48
L	Substrate Length	39
GW	Ground Width	31
GL	Ground Length	39
RTR	Right side truncate	4.59
LTR	Left side truncate	6.00
LSTL	Left Stub Length	7.00
RSTL	Right Stub Length	6.00
LSTW	Left Stub Width	4.00
RSTW	Right Stub Width	4.00
SL	U slot Antenna Length	7.50
SW	U slot Antenna Width	7.00
IL	Inset cut Length	6.00
IW	Inset cut Width	1.00
FL	Feed Length	12.00
FW	Feed Width	3.08

3. Results and Discussion

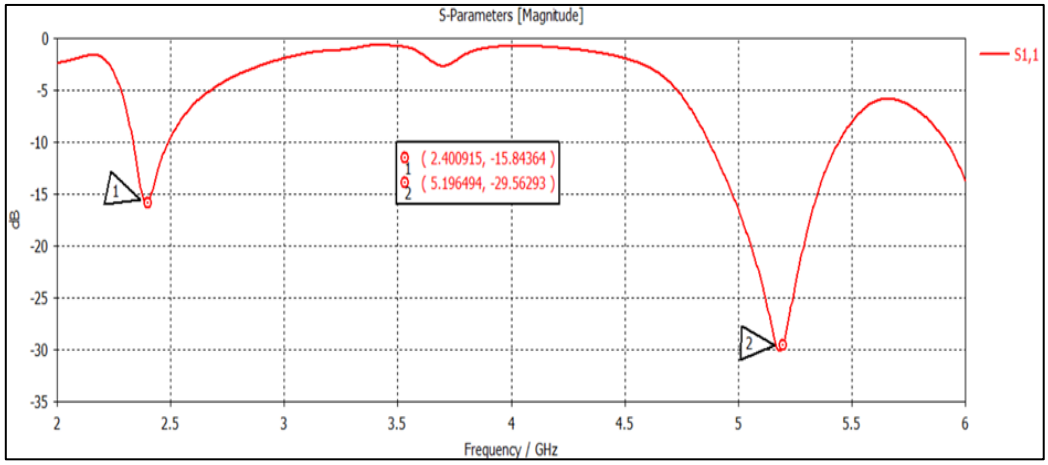

Figure 2. Return Loss Graph for 2.4 and 5.2 GHz

The response curve for the S_{11} magnitude shown in Figure 2 indicates the reflection characteristics of the antenna over the sweep frequency range from 2–6 GHz. Two distinct resonant dips can be seen at 2.40 GHz and 5.19 GHz, showing minimum values of −15.8 dB and −29.5 dB, respectively. Because the minima of both resonances are lower than the

generally accepted value of −10 dB matching level, the energy supplied to the antenna is effectively transferred into the radiated field without reflections towards the generator [18]. The presence of both resonances confirms the efficient use of the U-slot and truncated corners method to create two independent resonance modes. On the practical side, the first frequency (2.4 GHz) is ideal for transmitting low-rate telemetry data to the drone control station, while the latter (5.2 GHz) is good enough for transferring video streams from a UAV [19]. VSWR plot depicted in Figure 3 also supports the findings of impedance matching through the S_{11} parameters. It is noted that minimum VSWR values of 1.38 at 2.39 GHz and 1.06 at 5.18 GHz are achieved and meet the threshold value set by the industry of 2.0. Such values show near-perfect efficiency in power delivery from the transmission line to the radiating element, whereby very little incident power is reflected back [20]. They all tally with those of the S_{11} plot and therefore establish reliable dual band impedance characteristics.

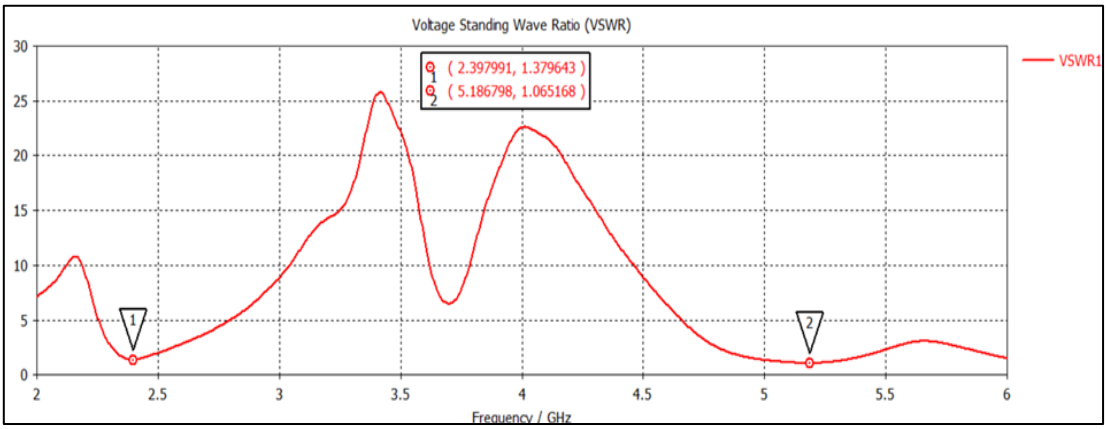

Figure 3. VSWR Graph for 2.4 and 5.2GHz

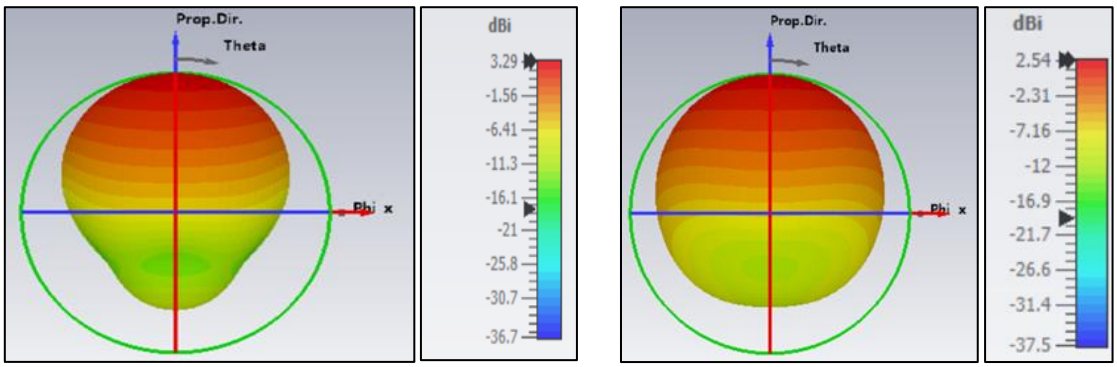

(a) (b)

Figure 4. 3D Radiation Patterns Representing the Antenna's Peak Gain Behaviour of (a) 2.4GHz & (b) 5.2GHz

The simulated far field three-dimensional gain patterns for the two operational frequencies can be seen in Figure 4 The maximum realized gains achieved at the two frequencies are 3.29 dBi at 2.4 GHz and 2.54 dBi at 5.2 GHz respectively, with broadside radiation taking place in both cases. The gains obtained correspond to the gains achieved by single layer patch antennas on lossy substrates like FR-4 and are sufficient for short to medium range telemetry applications in UAVs [21]. Broadside radiation is adequate for providing reliable telemetry, control command uplinks, and downlinking of sensed data in real time.

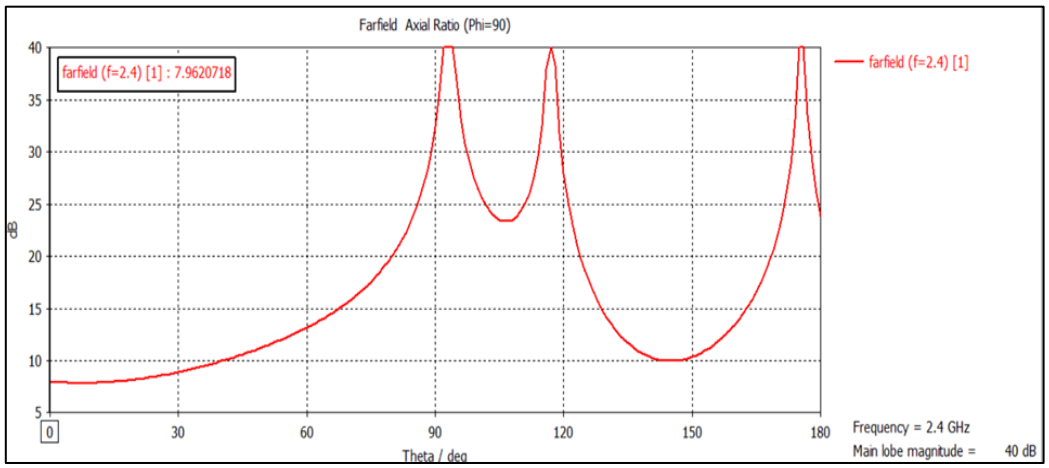

Figure 5. Axial Ratio for 2.4GHz

The angular distribution of far-field axial ratio (AR) in Figures 5 and 6 was determined at the frequencies of 2.4 GHz and 5.2 GHz, respectively. With reference to Figure 5, corresponding to the operating frequency at a lower level, the maximum calculated AR value is 7.96 dB and surpasses the 3 dB CP threshold limit. It is, therefore, concluded that the operation is not circular polarization but is either elliptical or linear polarization [22].

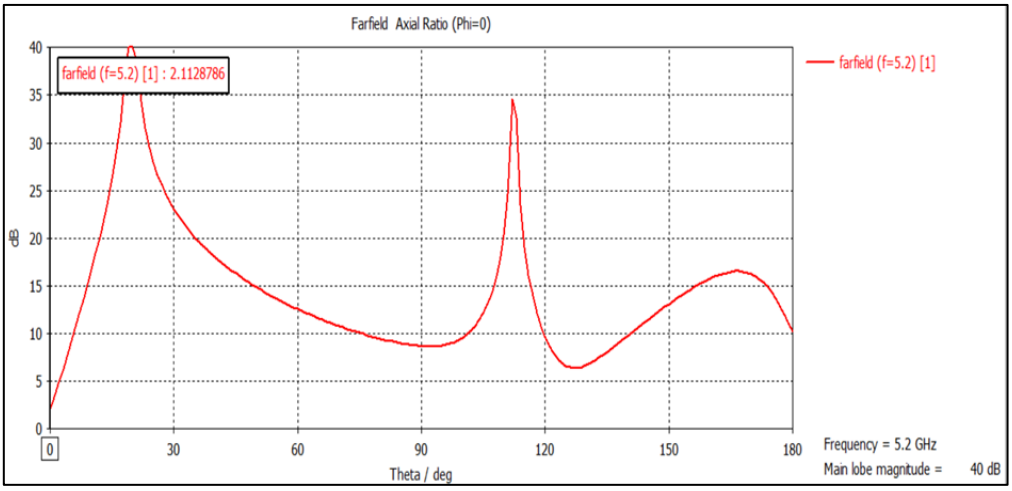

Figure 6. Axial Ratio for 5.2 GHZ

The reason for this scenario is related to the partial separation of orthogonal TM modes at the lower frequency, and the corner truncation structure by itself does not satisfy the requirement of balanced mode amplitude with 90 degrees phase difference. For the operating frequency at 5.2 GHz (Figure 6), however, the value of AR becomes 2.11 dB, suggesting that CP operation is achieved. The reason behind this is that at a higher operating frequency, the slot geometry is complemented by the perturbation structure for CP generation.

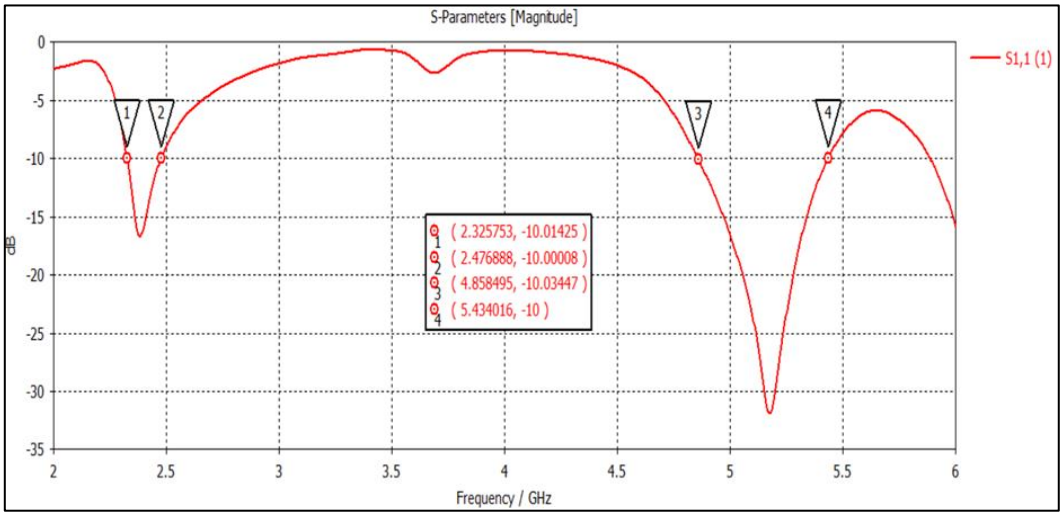

Figure 7. Bandwidth for 2.4 and 5.2 GHZ

Impedance bandwidth is determined by the range of frequencies for which the value of S_{11} is less than or equal to the matching limit of −10 dB. According to Figure 7, the lower operating band ranges from 2.32 GHz to 2.47 GHz, thus resulting in an impedance bandwidth of 150 MHz with a center frequency of 2.4 GHz. In the upper operating band, the range is between 4.8 GHz and 5.4 GHz, giving rise to an impedance bandwidth of 600 MHz.

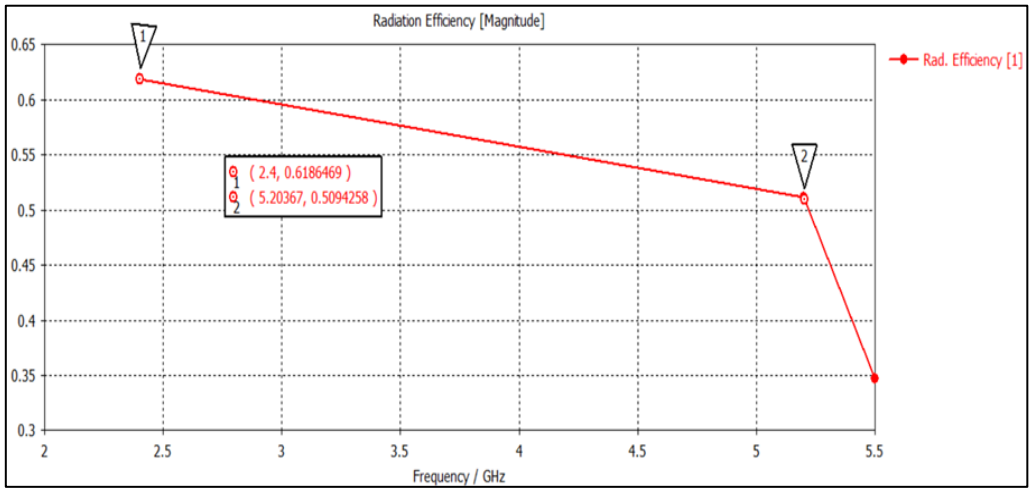

Figure 8. Radiation Efficiency for 2.4 and 5.2 GHZ

Efficiency of the proposed antenna simulation has been graphically depicted in Figure 8 between the frequency ranges of 2-5.5 GHz. Efficiency of the antenna stands to be 61.8% at 2.4 GHz and 50.9% at 5.2 GHz. Decrease in efficiency due to frequency increase is attributed to high loss tangent due to high frequency of FR-4 along with the addition of ohmic losses caused by copper metallization as well as current path deformation caused by the U-slot and perturbation elements. However, even in this case, both the efficiencies are deemed acceptable for the intended UAV application. Performance Evaluation of the Proposed Antenna & Existing Designs is presented in table 2.

Table 2. Performance Evaluation

Ref	Dimensions (mm)	Operating Frequency (GHZ)	Substrate	Bandwidth (MHz)
[13]	29 × 26 × 1.6	2.4,5	FR-4	140,552
[14]	44 × 41 × 1.6	2.4,5.2	FR-4	115,110
[15]	20 × 25 × 1	2.4,5.2	FR-4	80,650
[4]	40 × 40 × 1.6	2.4,5	FR-4	124,478
Proposed work	48 × 39 × 1.6	2.4,5.2	FR-4	163,600

4. Antenna Fabrication and Experimental Validation

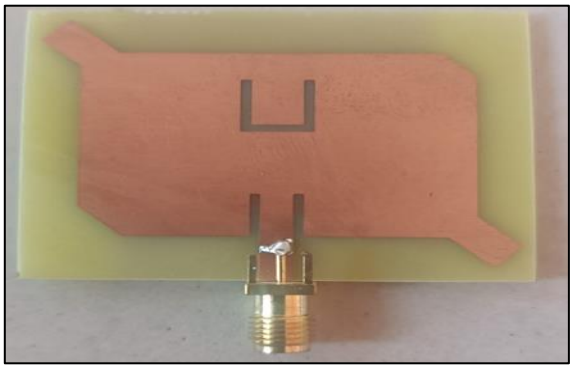

Figure 9. Antenna Top View

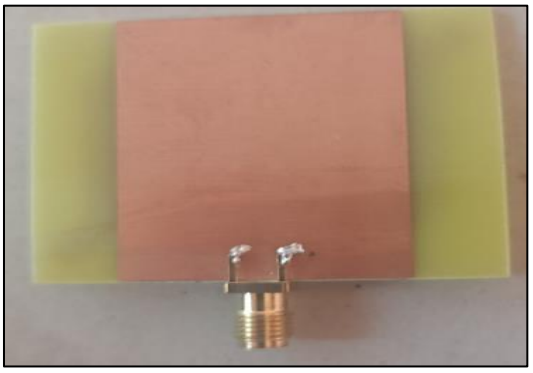

Figure 10. Antenna Back View

Two photographs of fabricated prototype are presented in Figure 9 and Figure 10. Antenna prototype was designed using an FR-4 laminate substrate, having a relative permittivity of $\varepsilon_r = 4.4$, dielectric loss tangent of 0.02, and a constant thickness of 1.6 mm. Dimensions of the total PCB board are 48×39 mm², which include the radiating patch region on the top side and the partial ground plane region on the back side, designed for dual band applications operating at 2.4 GHz and 5.2 GHz frequencies. Copper layout was created using

conventional UV-contact photolithography process followed by etching to accurately create patch and feed structures. For connecting the prototype, SMA 50 Ω edge-launched connector was mounted at the edge-launch port of the microstrip line by using reflow solder technique.

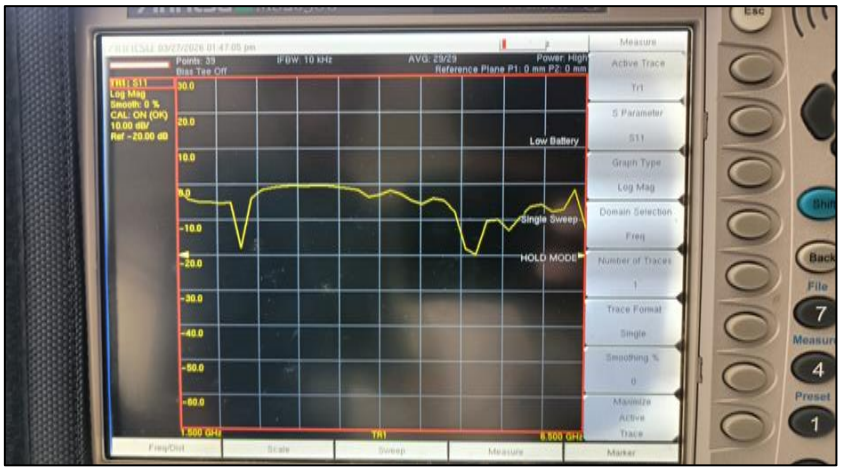

Figure 11. Measured Return Loss of the Fabricated Antenna using VNA

RF characterization of the prototype was conducted using an Anritsu vector network analyser, calibrated to the SMA connector reference plane using a full one-port SOLT calibration kit. The S_{11} parameter was recorded across the 1–6 GHz frequency range to assess the impedance matching behaviour of the fabricated antenna. Measurement results reveal resonance dips at 2.4 GHz and 5.2 GHz with minimum S_{11} values of −11 dB and −25 dB, respectively as shown in Figure 11. The −11 dB value at 2.4 GHz confirms acceptable impedance matching with manageable reflected power, while the −25 dB depth at 5.2 GHz indicates highly efficient power coupling into the antenna at the upper band.

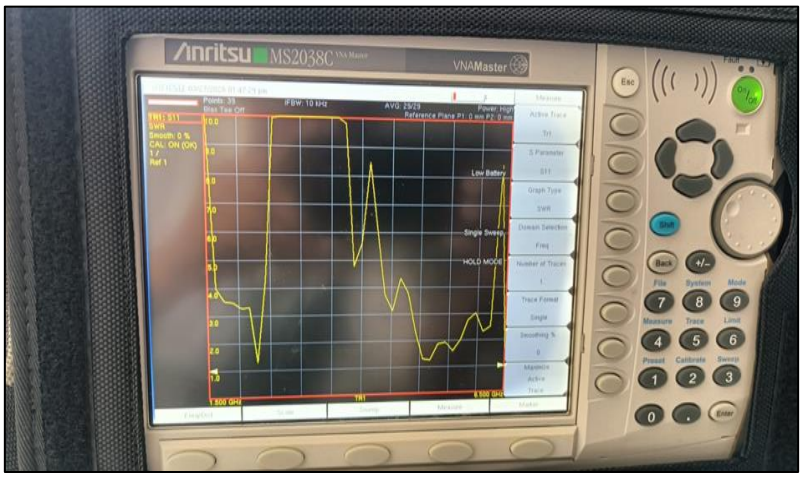

Figure 12. Measured VSWR of the Fabricated Antenna using VNA

The VSWR performance of the fabricated antenna is obtained from the measured S_{11} data across the frequency range of 2–6 GHz. The observed VSWR values are approximately 1.5 at 2.4 GHz and 1.8 at 5.2 GHz (figure 12). Since both values are below the acceptable limit of 2, the antenna demonstrates satisfactory impedance matching and effective power transfer with low signal reflection.

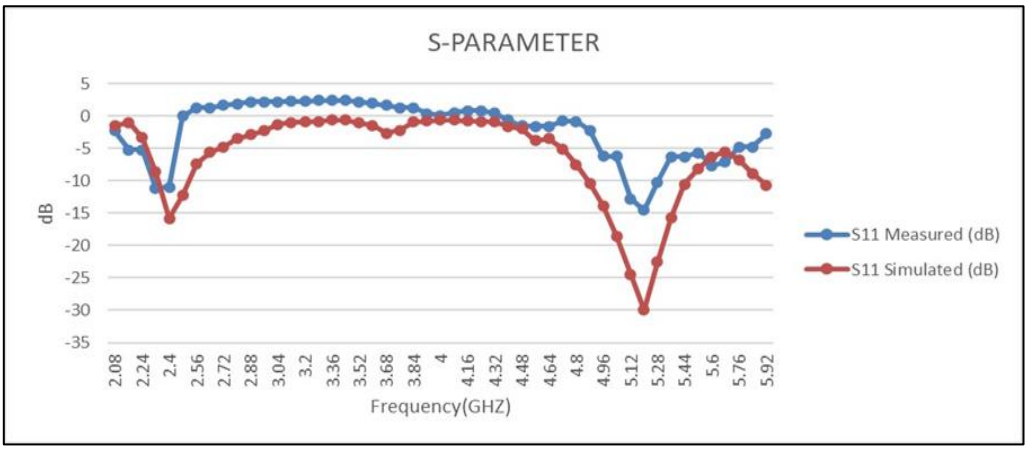

Figure 13. Simulated and Measured Return Loss in dB for 2.4 and 5.2 GHZ

The results of the simulated and measured S_{11} are shown together in Figure 13 to make an easy comparison between them possible. Resonances of -15 dB at 2.4 GHz and -29 dB at 5.2 GHz have been found in simulations, compared to measurements of -11 dB and -25 dB at the corresponding frequencies. All four measurements fall below the -10 dB matching limit, which indicates good matching both in simulation and in the actual antenna. A difference between the two traces is reasonable for the known reasons of inaccurate measurements such as etch tolerance, deviation from FR-4 datasheet values, and the presence of parasitic elements connected to SMA connectors.

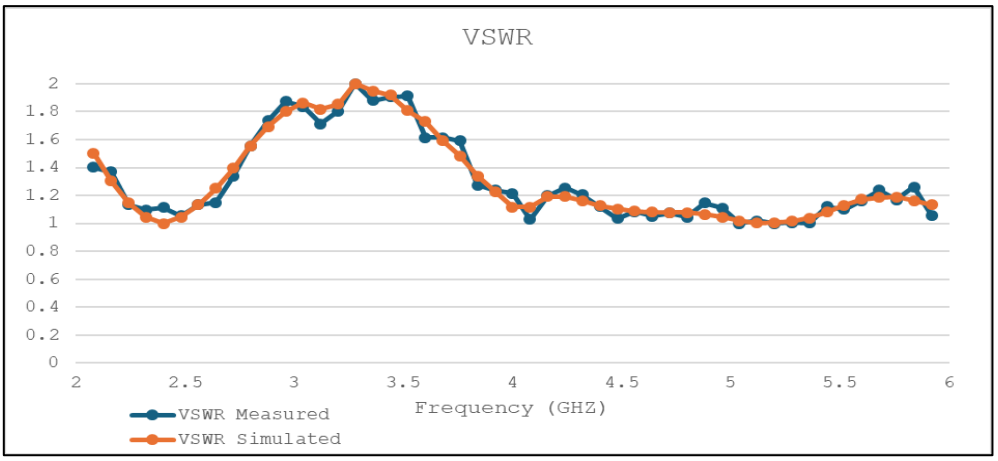

Figure 14. Simulated and Measured VSWR for 2.4 and 5.2 GHZ

In Figure 14, the simulated and measured VSWR plots for the two working bands have been shown in comparison. The simulated values of the VSWR are 1.2 at 2.4 GHz and 1.4 at 5.2 GHz, while their measured values are 1.5 and 1.8 respectively. In all these cases, the VSWR is less than 2.0, indicating low-reflection impedance matching in the case of both antennas. This indicates that the electromagnetic model adopted and the simulated antenna behavior is quite accurate, as reflected by the results obtained experimentally as well.

5. Conclusion

The current study has described the design, simulation, manufacturing, and testing of a miniature dual-band microstrip patch antenna intended for use in UAV communication onboard systems. Impedance matching was found to be satisfactory for the designed antenna at both frequencies of interest, 2.4 GHz and 5.2 GHz; a good match was observed between the simulation and measurement results for both bands, providing dual-band functionality verification. Circular polarization has been successfully realized at the frequency of 5.2 GHz, producing an axial ratio of 2.11 dB due to the use of both U-slots and corner perturbations. An axial ratio of 7.96 dB, corresponding to elliptic polarization, has been obtained at 2.4 GHz. Gains and radiation efficiencies of the antenna have been found to be appropriate for short-medium range UAV communication purposes in a cost-effective, small size, and FR-4 substrate-based design. Antenna performance appears to be highly dependent upon a proper compromise between geometries of slots, corners, and stubs. Further investigations should include developing a design capable of achieving circular polarization in both bands, increasing gains via antenna arrays and metasurfaces usage, realizing reconfigurations via PIN/varactor diodes, and testing antenna performances in actual UAV applications.

References

[1] Yang, X., Y. Qi, B. Yuan, Y. Cao, and G. Wang. “A Miniaturized High-Gain Flexible Antenna for UAV Applications.” International Journal of Antennas and Propagation 2021, vol. 2021: 9919425.

[2] Niyamanon, S., R. Senathong, and C. Phongcharoenpanich. “Dual-Frequency Circularly Polarized Truncated Square Aperture Patch Antenna with Slant Strip and L-Shaped Slot for WLAN Applications.” International Journal of Antennas and Propagation 2018, vol. 2018: 7684742.

[3] Yang, Y.-L., and D.-B. Lin. “A Compact Planar Wi-Fi Antenna with Optimized Radiation Patterns for Small UAV Applications.” Applied Sciences 2023, vol. 13: 7470.

[4] Almehmadi, A. S., and R. W. Aldhaheri. “A Novel Design of Dual-Band Circularly Polarized Microstrip Patch Antenna for Unmanned Aerial Vehicle Applications.” Applied Sciences 2023, vol. 13, no. 6, 1–15.

[5] Dhananjeyan, R., S. Ramesh, and D. Rajesh Kumar. “Performance Analysis of Eight-Element MIMO Mobile Phone Antenna for Sub-6 GHz 5G Applications.” Applied Computational Electromagnetics Society (ACES) Journal 2024, vol. 39, no. 4, 319–326.

[6] Mohammed, A. H., F. M. Alnahwi, and Y. I. A. Al-Yasir. “A Circularly Polarized Microstrip Antenna with Dual Circular Polarization Using a 90° Hybrid Coupler and Proximity-Coupled Feeding for LTE 43 5G Applications.” Applied Sciences 2024, vol. 14: 11877.

[7] Kayalvizhi, K., and S. Ramesh. “A Novel MIMO Antenna with Switchable UWB/5G Modes for Vehicular Terminals.” Microwave and Optical Technology Letters 2023, vol. 65, no. 9, 2640–2645.

[8] Kandregula, V. R., Z. D. Zaharis, Q. Z. Ahmed, F. A. Khan, T. H. Loh, J. Schreiber, A. J. R. Serres, and P. I. Lazaridis. “A Review of Unmanned Aerial Vehicle Based Antenna and Propagation Measurements.” Sensors 2024, vol. 24: 7395.

[9] Ray, M. K., and K. Mandal. “Pair of Diagonal Slots Loaded Low-Profile Circularly Polarised Patch Antenna with Wide 3 dB Axial Ratio Beamwidth.” IET Microwaves, Antennas & Propagation 2019, vol. 13, 2433–2438.

[10] Jin, H., C.-Z. Han, Y. Fu, and H. Yang. “A Low-Profile Dual-Band Directional Antenna for Unmanned Aerial Vehicle Applications.” International Journal of Antennas and Propagation 2022, vol. 2022, no. 1, 4765008.

[11] Ebenezer Abishek, R., S. Ramesh, R. Parthasarathy, and E. Manikandan. “Low-Profile Circularly Polarized Conformal Antenna Array with Side Lobe Suppression for Vehicular SATCOM Applications.” Applied Computational Electromagnetics Society (ACES) Journal 2023, vol. 38, no. 6, 439–447.

[12] Şahin, D. A., and A. Kaya. “2.4 GHz and 5 GHz Dual Band Wi-Fi Antenna Design for IoT Based Smart Media Application.” European Journal of Science and Technology 2022, no. 39, 17–20.

[13] Li, X.-P., C.-L. He, J.-F. Ji, M.-B. Yang, Y. Zhang, A.-X. Zhang, and W. Li. “A Compact Broadband Common-Aperture Dual-Polarized Antenna for Drone Applications.” Micromachines 2024, vol. 16: 48.

[14] Saturday, J. C., K. M. Udofia, and A. J. Jimoh. “Design of Dual Band Microstrip Antenna Using Reactive Loading Technique.” Mathematical and Software Engineering 2016, vol. 2, no. 2, 114–121.

[15] Zhuo, Y., L. Yan, X. Zhao, and K. Huang. “A Compact Dual-Band Patch Antenna for WLAN Applications.” Progress in Electromagnetics Research Letters 2011, vol. 26, 15–24.

[16] Ahmad, Mansoor, and Fazli A. Khalil. “Design and Fabrication of a 2.4 GHz Right Hand Circular Polarized Micro-Strip Patch Antenna.” Proceedings of the Pakistan Academy of Sciences: A. Physical and Computational Sciences 2021, vol. 58, no. 4, 1–10.

[17] Gour, Sonam, Geetika Mathur, and Amit Rathi. “A Miniaturized Dual Band Rectangular Stripped Design of Microstrip Patch Antenna.” International Conference on Next Generation Communication & Information Processing (INCIP) 2025, 834–837,

[18] Ye, Hong Chuan, Chunxu Mao, Ling Liang Dai, and Xiu Yin Zhang. "Dual-band dual-polarized antenna and array with enhanced bandwidth for 5g millimeter-wave applications." IEEE Antennas and Wireless Propagation Letters 2025, vol. 24, no. 7, 1829-1833

[19] Gopinath, D., and P. Marichamy. "On the design and analysis of multi-band micro-strip patch antenna for wireless body area network applications." EURASIP Journal on Wireless Communications and Networking 2025, no. 1, 13.

[20] Hassan, Sahar K., and Zaid M. Khudair. "Innovative Dual-Band Microstrip Patch Antenna Design for Enhanced Wireless Communications." In International Conference on Emerging Trends in AI and Computational Technologies, Cham: Springer Nature Switzerland, 2024, 238-248.

[21] Balanis, Constantine A. Antenna theory: analysis and design. John wiley & sons, 2016.

[22] Zhao, Z., F. Liu, J. Ren, Y. Liu, and Y. Yin. “Dual-Sense Circularly Polarized Antenna with a Dual-Coupled Line.” IEEE Antennas and Wireless Propagation Letters 2020, vol. 19, no. 8, 1415–1419.